Pergamon

Int. Comm. Heat Mass Transfer, Vol. 28, No. 5, pp. 605–616, 2001

0735-1933/01/$–see front matter

PII: S0735-1933(01)00265-2

EXPERIMENTAL AND NUMERICAL STUDY OF MICROWAVE DRYING IN UNSATURATED POROUS MATERIAL

Phadungsak Ratanadecho, K. Aoki and M. Akahori
Nagaoka University of Technology
1603-1, Kamitomioka, Nagaoka
Niigata, Japan , 940-2188

(Communicated by C.L. Tien and A. Majumdar)

ABSTRACT

The drying of unsaturated porous material due to microwave drying (2.45GHz) has been investigated numerically and experimentally. Most importantly, this work focuses on the influence of moisture content on each mechanism (vapor diffusion and capillary flow) during microwave drying process. Based on a model combining the electric field and heat-mass transport equations show that the variation of initial moisture content and particle size changes the degree of penetration and rate of absorbed energy within the material. The small bead size leads to much higher capillary forces resulting in a faster drying time.

Introduction

Intensive microwave drying has been studied by recent literatures (Jolly et al. [1], Jansen et al. [2], Wei et al. [3], Schundler [4], Turner et al. [5], Constant et al. [6], Adu et al. [7], Perre et al. [8], Monzo-Cabrera et al. [9] and Ratanadecho et al. [10]). However, a little effort has been reported on study of the influence of the variation of initial moisture content and particle sizes on each mechanism (vapor diffusion and capillary flow) during microwave drying process. Additionally, a full comparison of the space-time evolution of the temperature and moisture content between mathematical simulation results with experimental drying data has not been systematically studied.

In general, during microwave drying process of capillary porous material from the early drying times through the longer drying times, the phenomenon is too complex for the theoretical explanation due to the strongly effects of dielectric properties on the overall drying kinetics. Furthermore, from macroscopic point of view, the effects of the irradiation time, particle sizes and the variation of initial moisture content on each mechanisms and microwave energy absorption within capillary porous material must be clarified in detail. This study reports a comparison of simulation based on a one-dimensional model with experimental measurement in which the microwave operating at a frequency of 2.45GHz is

employed. The effects of the irradiation time, particle sizes and the variation of initial moisture content on microwave drying kinetics are clarified in this work. The result presented here provides a basis for fundamental understanding of microwave drying of capillary porous material.

Experimental Apparatus

Figure 1 shows the experimental apparatus for the drying system. A domestic microwave oven was modified to give a steady and continuous power at a microwave frequency of 2.45GHz, it is transmitted along the x-direction of the cylindrical test section with inner diameter of 40 mm and height of 130 mm toward a water load that is situated at the end of the cylindrical test section. The water load ensures that only a minimal amount of microwave is reflected back to the sample. The sample (capillary porous packed bed) studied is an initially unsaturated packed bed, which is composed of glass beads, water and air. It is inserted in the cylindrical test section. The aluminum foil is wrapped around the outside wall of cylindrical test section to protect any incident wave from the circumferential plan, the outside wall of aluminum foil is covered with insulation to reduce the heat loss. During the experiment, the temperature distributions in the sample were measured with lightfiber sensor.

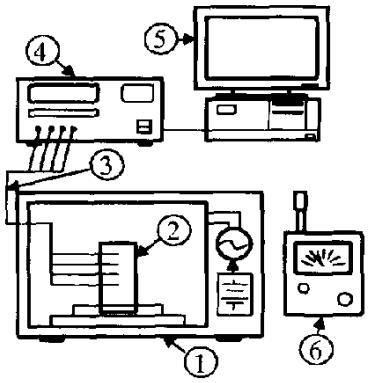

FIG. 1
Experimental apparatus

Analysis of Microwave Drying Process

The Rate of Volumetric Heat Generation Due to Absorption of Microwave

Figure 2 shows the analytical model for microwave drying of the sample. The rate of volumetric energy absorbed may be derived from the microwave power propagated through a sample with attenuation constant, and can be written in final form as:

$$Q = -\frac{\partial P}{\partial x}dx = 2\alpha P dx = 2\alpha dx.2\pi f\varepsilon\left(\tan\delta\right)E^2 e^{-2\alpha x} \tag{1}$$

where α is the attenuation constant which can be calculated from:

$$\alpha = 2\pi f \sqrt{\frac{\varepsilon_0 \varepsilon_r \mu_0}{2}} \left(\sqrt{\tan^2\delta + 1} - 1\right) = \frac{2\pi f}{c} \sqrt{\frac{\varepsilon_r}{2}} \left(\sqrt{\tan^2\delta + 1} - 1\right) \quad (2)$$

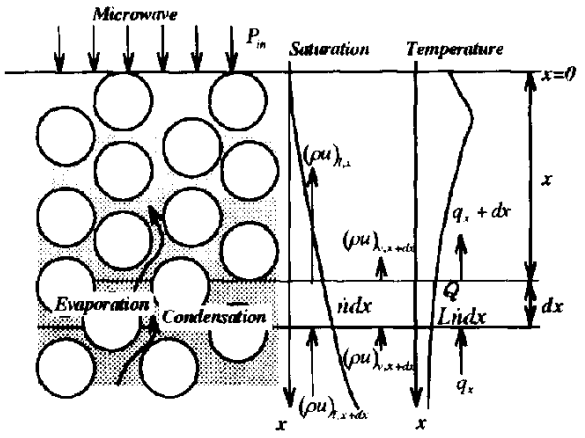

FIG. 2
Analytical model

The attenuation parameter (α) controls the rate at which the incident field decays, and is inversely proportional to the skin depth, i.e., $\alpha = 1/\delta_s$. In this work, the effects on the overall drying kinetics are examined by selecting the dielectric properties as a function of water saturation (moisture content) and temperature. In order to determine the functional dependence of the combination of water saturation and temperature, the theory mixing formulas is used [11], in which the volume fractions (υ) of water, water vapor and glass particle were each considered, as follows:

$$\varepsilon(s,T) = \left(\varepsilon'(s,T) - j\varepsilon''(s,T)\right) \quad (3a)$$

where

$$[\varepsilon'(s,T)]^m = \sum_{i=1}^{3} \upsilon_i [\varepsilon_{ri}'(T)]^m = \phi s[\varepsilon_{rl}'(T)]^m + \phi(1-s)[\varepsilon_{ra}']^m + (1-\phi)[\varepsilon_{rp}']^m \quad (3b)$$

$$[\varepsilon''(s,T)]^m = \sum_{i=1}^{3} \upsilon_i [\varepsilon_i''(T)]^m = \phi s[\varepsilon_{rl}''(T)]^m + \phi(1-s)[\varepsilon_{ra}'']^m + (1-\phi)[\varepsilon_{rp}'']^m \quad (3c)$$

in which the parameter m in this equation is likely to vary over the range 0-1, as suggested by Wang and Schmugge[11]. The loss tangent coefficient can be expressed as follow:

$$\tan\delta = \frac{\varepsilon''}{\varepsilon'} \quad (3d)$$

Figure 3 depict the graphical representation of the dielectric properties by using formula (3a-3d) for capillary porous material, where the dielectric properties for the water are taken from Von Hippel [12] to depend on temperature and for the gas phase, to be constant. However again, some numerical values for skin depth, relative permittivity and loss tangent at various moisture content are listed in Table 1.

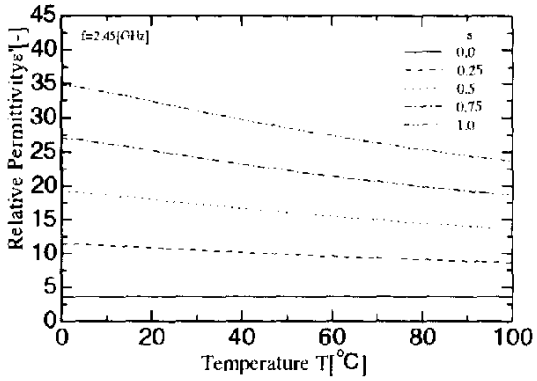

FIG.3(a)
Relative permittivity

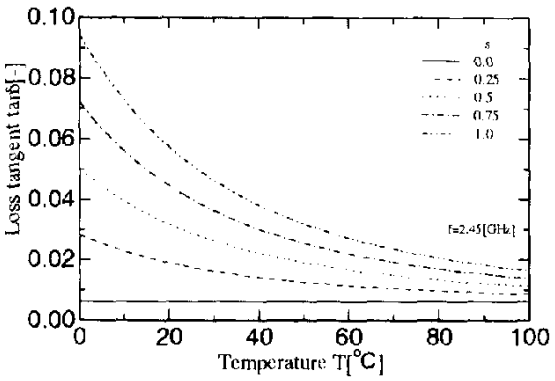

FIG.3(b)
Dielectric loss coefficient

TABLE 1

Dielectric properties of the sample (Corresponding to: T=20[℃] and f=2.45GHz)

Moisture Content (s)	Relative Permittivity (ε_r')	Loss Tangent ($\tan\delta$)	Skin depth (δ_s)
0.0	3.5420	0.0062	3.338119
0.25	10.9606	0.0190	0.607039
0.5	18.3110	0.0319	0.285429
0.75	25.6955	0.0447	0.171784
1.0	33.0801	0.0589	0.117645

Analysis of Heat and Mass Transport

The main transport mechanisms that enables moisture movement during microwave drying of the sample are: liquid flow driven by capillary pressure gradient and gravity while the vapor is driven by the gradient of the partial pressure of the evaporating species. The main assumptions involved in the formulation of the transport model are:

1. The capillary porous material is rigid. No chemical reactions occur in the sample.
2. Local thermodynamics equilibrium is assumed.
3. Simultaneous heat and mass transport occurs at constant pressure, where the dominant mechanisms are capillary transport, vapor diffusion and gravity. Such is generally the case in drying of capillary porous medium at atmospheric pressure when the temperature is lower than the boiling point [10].

4. Corresponding to electric field, temperature and moisture profiles also can be assumed to be one-dimensional form.
5. The non-thermal effect of microwave irradiation is neglected.

Mass conservation The macroscopic mass conservation for liquid and water vapor are written as:

Liquid phase
$$\rho_l \phi \frac{\partial s}{\partial t} + \rho_l \frac{\partial u_l}{\partial x} = -\dot{n} \tag{4}$$

Vapor phase
$$\frac{\partial}{\partial t}\{\rho_v \phi(1-s)\} + \frac{\partial}{\partial x}[\rho_v u_v] = \dot{n} \tag{5}$$

Energy conservation The temperature of the sample exposed to irradiation is obtained by solving the conventional heat transport equation with the microwave energy absorbed included as a local heat generation term. The governing energy equation describing the temperature rise in the sample is the time dependent equation is

$$\frac{\partial}{\partial t}\left[(\rho c_p)_T T\right] + \frac{\partial}{\partial x}\left[\left\{\rho_l c_{pl} u_l + (\rho_a c_{pa} + \rho_v c_{pv}) u_g\right\} T\right] + H_v \dot{n} = -\frac{\partial q}{\partial x} + Q \tag{6}$$

Phenomenological relations The expressions for the superficial average velocity of the liquid and gas phases, the generalized Darcy's law in the following form is used:

$$u_l = -\frac{KK_{rl}}{\mu_l}\left[\frac{\partial p_g}{\partial x} - \frac{\partial p_c}{\partial x} - \rho_l g\right], \quad u_g = -\frac{KK_{rg}}{\mu_g}\left[\frac{\partial p_g}{\partial x} - \rho_g g\right] \tag{7}$$

where μ_l and μ_g denote the viscosity of liquid and gas phases, respectively.

For the velocity of water vapor and air phases, the generalized Fick's law in the following form is used:

$$\rho_v u_v = \rho_v u_g - \rho_g D_m \frac{\partial}{\partial x}\left(\frac{\rho_v}{\rho_g}\right), \quad \rho_a u_a = \rho_a u_g - \rho_g D_m \frac{\partial}{\partial x}\left(\frac{\rho_a}{\rho_g}\right) \tag{8}$$

where the capillary pressure (p_c) is related to the gas and liquid phases can be written by

$$p_c = p_g - p_l \tag{9}$$

and D_m is the effective molecular mass diffusion [13] can be written by

$$D_m = \frac{2\phi}{3-\phi}(1-s)D \tag{10}$$

Equilibrium relations A typical set of constitutive relationships for liquid and gas systems in empirical forms [13] given by:

$$k_{rl} = s_e^3, \quad k_{rg} = 1.2984 - 1.9832 s_e + 0.7432 s_e^2 \tag{11}$$

where s_e is the effective water saturation considered the irreducible water saturation (s_{ir}=0.06) and defined by:

$$s_e = \frac{s - s_{ir}}{1 - s_{ir}} \tag{12}$$

The capillary pressure is further assumed to be adequately represented by Leverett's well know $J(s_e)$ functions, the relationship between the capillary pressure and the water saturation is defined by using Leverett functions $J(s_e)$:

$$p_c = p_g - p_l = \frac{\sigma}{\sqrt{K/\phi}} J(s_e) \tag{13}$$

in which σ is the gas-liquid interfacial tension, and Leverett functions given by:

$$J(s_e) = 0.325(1/s_e - 1)^{0.217} \tag{14}$$

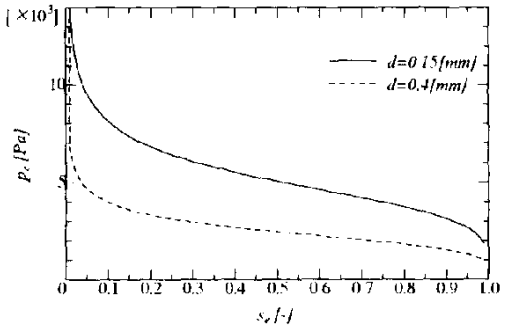

FIG. 4a
Typical relationship between, p_c and s_e

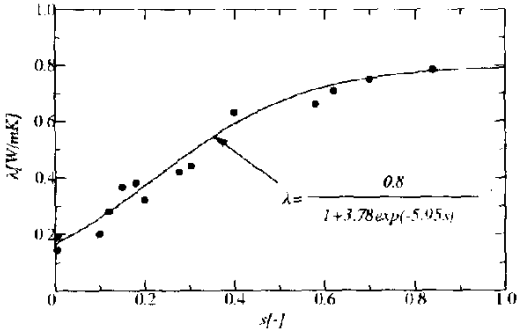

FIG. 4b
Effective thermal conductivity

Figure 4a shows the typical moisture characteristic curve (relationship between capillary pressure and water saturation) for different particle sizes obtained from present experiments. It is seen that, in the case of the same water saturation, a small particle size corresponds to a higher capillary pressure. The characteristic of water transport in porous material obtained here is shown in Table 2.

TABLE 2
The characteristic of water transport in porous material

Diameter, d [mm]	Porosity, ϕ [-]	Permeability, k [m^2]
0.15	0.385	8.41×10^{-12}
0.4	0.371	3.52×10^{-11}

Figure 4b, the effective thermal conductivity of the capillary porous medium is represented as a function of water saturation which can be written as:

$$\lambda = \frac{0.8}{1 + 3.78e^{-5.95s}} \tag{15}$$

State Equations The gas phase is assumed to be an ideal mixture of perfect gases, so that the species density can be determined by the state equations.

Moisture and heat transport equations After some mathematical manipulations, the system of two non-linear coupled partial differential equations, which govern the drying process are given by:

$$\phi \frac{\partial}{\partial t}\{\rho_l s + \rho_v(1-s)\} + \frac{\partial}{\partial x}\left[\rho_l \frac{KK_{rl}}{\mu_l}\left(\frac{\partial p_c}{\partial x} + \rho_l g\right) + \rho_v \frac{KK_{rg}}{\mu_g}(\rho_g g) - D_m \frac{\partial \rho_v}{\partial x}\right] = 0 \tag{16}$$

$$\frac{\partial}{\partial t}\left[(\rho c_p)_T T\right] + \frac{\partial}{\partial x}\left[\{\rho_l c_{pl} u_l + (\rho_a c_{pa} + \rho_v c_{pv}) u_g\} T\right] + H_v n = \frac{\partial}{\partial x}\left[\lambda \frac{\partial T}{\partial x}\right] + Q \tag{17}$$

where $$(\rho c_p)_T = \rho_l c_{pl} \phi s + ((\rho c_p)_a + (\rho c_p)_v)\phi.(1-s) + \rho_p c_{pp}(1-\phi) \tag{18}$$

$$n = \frac{\partial}{\partial t}\{\rho_v \phi(1-s)\} + \frac{\partial}{\partial x}\left[\rho_v \frac{KK_{rg}}{\mu_g}\rho_g g - D_m \frac{\partial \rho_v}{\partial x}\right] \tag{19}$$

Boundary and initial conditions

The boundary conditions proposed for the open boundary of the sample, for the exchange of energy at the open boundary can be described in the following form:

$$-\lambda \frac{\partial T}{\partial x} = h_c(T - T_a) + n H_v \tag{20}$$

$$\rho_l u_l + \rho_v u_v = h_m(\rho_v - \rho_{v\infty}) \tag{21}$$

where h_c is the heat transfer coefficient , h_m is the mass transfer coefficient, ρ_{vs} is the density of water vapor at the open boundary and $\rho_{v\infty}$ is reference vapor density in the gas phase surrounding the open boundary. Considering the boundary conditions at the closed boundary (symmetry-impermeable) that no heat and mass exchange take place:

$$\frac{\partial T}{\partial x} = 0, \quad \frac{\partial u}{\partial x} = 0 \tag{22}$$

Numerical Procedure

Concerning the system of nonlinear partial differential equations (Eqs.(16)-(22)) must be solved by the method of finite differences base on the notation of control volume as described by Patankar [14]. At each time increment, the nodal value of s and T were solved iteratively and convergence was checked on both variables. The Newton-Raphson method was employed at each iteration to quicker the convergence.

Results and Discussions

The experimental results for microwave drying of a capillary porous material were compared with mathematical model simulations. However, all processes using the electric field intensity of 2800 V/m, initial temperature of 15 ℃ and ambient temperature of 15 ℃ were selected.

Some of electromagnetic and thermo-physical properties used in the computation are given in Table 3.

TABLE 3

The electromagnetic and thermo-physical properties used in the computations

$\varepsilon_0 = 8.85419\times10^{-12}$[F/m]	$\mu_0 = 4.0\pi\times10^{-7}$[H/m]	
$\varepsilon_{ra} = 1.0$	$\varepsilon_{rp} = 5.1$	
$\mu_{ra} = 1.0$	$\mu_{rp} = 1.0$	$\mu_{rl} = 1.0$
$\tan\delta_a = 0.0$	$\tan\delta_p = 0.01$	
$\rho_a = 1.205$[kg/m^3]	$\rho_p = 2500.0$[kg/m^3]	$\rho_l = 1000.0$[kg/m^3]
$c_{pa} = 1.007$[kJ/(kg·K)]	$c_{pp} = 0.80$[kJ/(kg·K)]	$c_{pl} = 4.186$[kJ/(kg·K)]
λ_a[W/(m·K)]	$\lambda_p = 1.0$[W/(m·K)]	$\lambda_l = 0.610$[W/(m·K)]

The temperature profile as a function of distance at various times is shown in Fig. 5, which correspond to that of initial moisture content of 0.5 and particle size of 0.15 mm. In contrast to that in conventional drying, microwave drying gives higher temperatures inside the drying sample while the surface temperature stays colder due to the cooling effect of ambient air. At the same time the evaporation takes place at the surface of the sample at a lower temperature due to evaporative cooling.

It is seen that the temperature profile within the sample rises up quickly in the early stage of the drying process, after that its rise slows down. This because the behavior of the dielectric loss coefficient decreases significantly with increasing temperature (as referred to Fig.3), the microwave energy absorbed can decrease at locations of higher temperature where the microwave configuration established inside the sample minimizes (Fig. 6). In Fig. 5, near the end stage of drying as the moisture content inside the sample is reduced, this decreases the microwave energy absorbed. Thus, equilibrium is reached between microwave drying and convective losses by lowering the product temperature. The simulated results are in agreement with the experimental results for microwave drying.

Figure 7 shows the moisture profile within the sample. It can be seen that the moisture continuously decreased toward the surface and steadily declines with time. At the early stage of drying process, the surface of the sample is supplied with liquid water through gradient in the capillary pressure, and because of the condensation of water vapor (which moves towards the surface due to a gradient in the vapor partial pressure), due to the lower temperature of the surface. However, the capillary flow plays an important role in the moisture migration mechanism for this stage, especially, in the case of higher initial moisture content (s_0=0.8). In Fig. 7, continued drying would eventually cause the average moisture content inside the sample to decrease and lead to decreased microwave energy absorbed (as referred to Fig.6), reduced the increasing of temperature and evaporation rate. At the longer drying times, the vapor

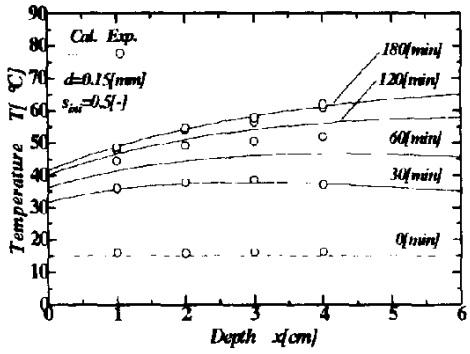

FIG. 5
Temperature profiles

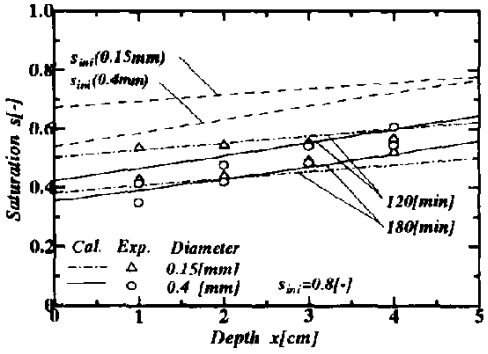

FIG. 8
Moisture profiles at various particle sizes

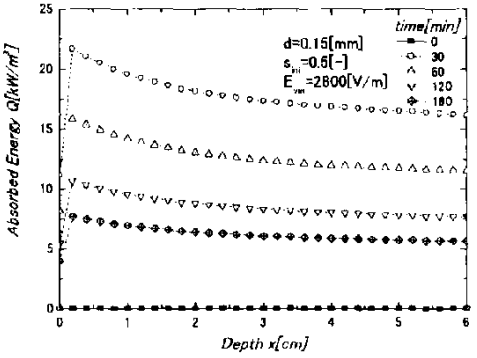

FIG. 6
Energy absorbed profiles

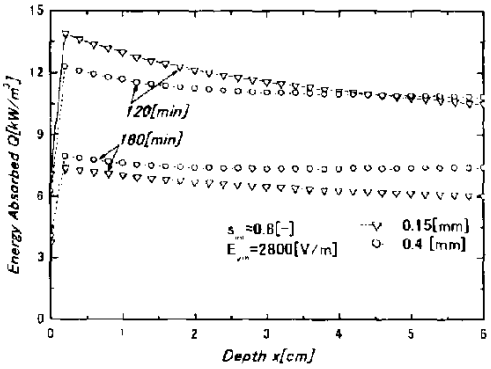

FIG. 9
Energy absorbed profiles at various particle sizes

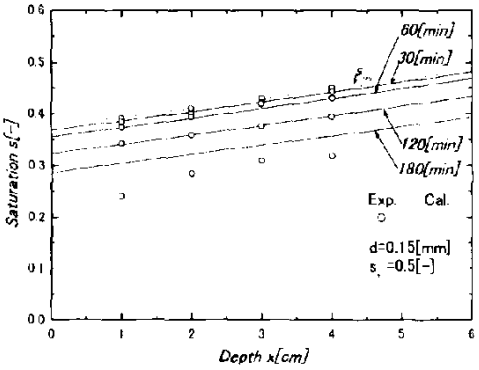

FIG. 7
Moisture profiles

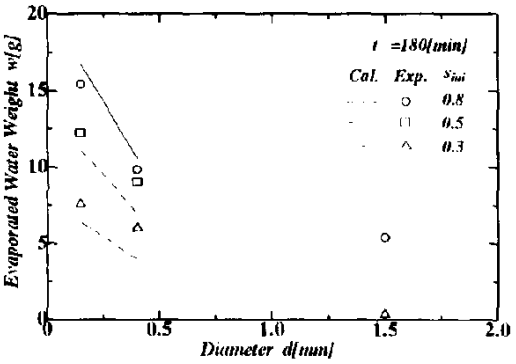

FIG. 10
Evaporated water weight vs. particle sizes

diffusion effect plays an important role in the moisture migration mechanism because of the sustained vaporization that is generated within the sample.

The following discussion refers to the effect of glass bead size under the same conditions. The moisture profiles and microwave energy absorbed profiles are shown in Figs. 8 and 9, respectively. Figure 8 shows the moisture profiles for two particle sizes (d=0.15mm and d=0.4mm), which correspond to that of initial moisture content of 0.8. The observed moisture profiles at the leading edge of the sample in the case of small particle size are higher than those in the case of larger particle size. This is because of the small particle size (which corresponds to a higher capillary force, as referred to Fig. 4) can cause moisture to reach the surface at a higher rate than that in the case of larger particle size; this corresponds to a greater amount of microwave energy absorbed (Fig. 9) at the leading edge of sample. Hence, even higher moisture content can lead to higher temperatures in this region.

Continued drying would eventually cause the average moisture content inside the sample to decrease and lead to decreased microwave energy absorbed. This phenomenon explains why the microwave energy absorbed within the sample in the end stage of drying (180 min) is slightly lower than that observed in the early stage of drying; this is more significant in the case of smaller particle size (Fig. 9).

The variation of the drying rate with time obtained by simulation is compared with the experimental results in Fig. 10. The small bead size, however, leads to much higher capillary forces resulting in a shorter drying time and more uniform moisture profile inside the sample. Furthermore, for a high moisture sample, as compared to the low moisture sample, rates of heating are higher and drying rate is much higher, due to the capillary flow plays an important role in the moisture migration mechanism for this sample. The simulated results are in good agreement with the experimental results.

The observation of moisture profiles depicted in Figs. 7 and 8 for the sample verifies that the match between the simulation results and experimental data is qualitatively consistent, with the simulation results exhibiting the same overall trend of the experimental profiles. However, the discrepancy may be attributed to uncertainties in the thermal and dielectric properties database. Additionally, The discrepancy may be attributed from the nonuniformity of the microwave irradiation during experimental process.

Finally, a more general observation concerning the moisture profiles for many materials pertains to the effect of matrix structure on the mechanism of moisture movement. From a macroscopic point of view, the ease with which the water can move in the liquid phase depends on the nature of the matrix structure within the porous material. In truly capillary porous material, a natural redistribution of the moisture from inside the material as the surface water evaporates. However, many materials have structures in which the pores are too large or too discontinuous for this to take place. In other materials, the water is held in a matrix which makes water liquid movement impossible.

Conclusions

The experiments and theoretically analysis presented in this work describe many of the important interactions within a capillary porous material during microwave drying. The following summarizes the conclusions of this work:

(1) A generalized mathematical model of drying by microwave oven is proposed. It is used successfully to describe the drying phenomena under various conditions.

(2) The effects of the irradiation time, particle sizes and the variation of initial moisture content on the microwave drying kinetics are clarified in detail, considering the influence of moisture content on each mechanism, as well as, the vapor diffusion and capillary flow.

(3) The small bead size leads to much higher capillary forces resulting in a faster drying time.

(4) Additionally, in this work the microwave energy absorbed was assumed to decay exponentially into the sample following the aid of Lambert's law. This assumption is valid for the large dimensions of sample used in study. For a small sample, the spatial variations of the electromagnetic field and microwave energy absorbed within sample must be obtained by a complete solution of the unsteady Maxwell's equations. Refer to Perre and Turner [8] and Ratanadecho et al. [10] for a detailed discussion.

Acknowledgment

The authors gratefully acknowledge the financial support provided under the Science Research Grant of the Japanese Ministry of Education, for the development of the experimental and simulation facilities described in this paper.

Nomenclature

C_p	specific heat capacity [J/kgK]	P	microwave power [W]
		p	pressure [Pa]
D_m	effective molecular mass diffusion [m^2/s]	Q	microwave energy absorbed [W/m^3]
		R	universal gas constant [J/mol/K]
c	light velocity [m/s]	s	water saturation [-]
E	electric field intensity [V/m]	T	temperature [°C]
f	frequency [Hz]	$\tan\delta$	loss tangent coefficient [-]
g	gravitational constant [m/s^2]	t	time [s]
k	permeability [m^2]	u	velocity [m/s]
n	phase change term [$kg/m^3 s$]		

Greek letters

ϕ	porosity [-]	λ	effective thermal conductivity [W/mK]
ρ	density [kg/m^3]	μ	magnetic permeability [H/m]
ε	permittivity [F/m]	δ_s	skin depth [m]

Subscripts

0	free space	r	relative
a	air	v	water vapor
c	capillary	l	liquid water
g	gas	x	coordinate axis [m]
p	particle		

References

1. P. Jolly and I.W. Turner, *J. Microwave Power and Electromagnetic Energy*, 25, 211 (1990).
2. W. Jansen and B. Wekken, *J. Microwave Power and Electromagnetic Energy*, 26, 2227 (1991).
3. C.K. Wei, H.T. Davis, E.A. Davis and J.T. Gordon, *AIChE J.*, 31, 842 (1985).
4. E.U. Schundler, *Trans IChemE*, 71, 622 (1993).
5. I.W. Turner and W.J. Furguson, *Drying Technology*, 13, 1477 (1995).
6. T. Constant, C. Moyne and P. Perre, *AIChE J.*, 42, 359 (1996).
7. B. Adu and L. Otten, *J. Microwave Power and Electromagnetic Energy*, 31, 2227 (1996).
8. P. Perre and I.W. Turner, *AIChE J.*, 10, 2579 (1997).
9. J. Monzo-Cabrera, A. Diaz-Morcillo, J.M. Catala-Civera, E. de los Reyes, *International Communication in Heat and Mass Transfer*, 27, 1101 (200).
10. P. Ratanadecho, K. Aoki and M. Akahori, *Drying Technology*, 18 (2001).
11. J. Wang and T. Schmugge, *IEEE Transactions on geosciences and remote sensing*, 4, 288 (1980).
12. A.R. Von Hippel, *Dielectric Materials and Applications*, MIT Press, Boston(1954).
13. M. Kaviany, *Principle of Heat Transfer in Porous Media*, Springer, Newyork (1991).
14. S.V. Patankar, *Numerical Heat Transfer and Fluid Flow*, Hemisphere, New York (1980).
15. K.G. Ayappa, *Review in Chemical Engg.*, 13, 1 (1997).

Received May 17, 2001